# On the 3-D Placement of Airborne Base Stations Using Tethered UAVs

Mustafa A. Kishk, *Member, IEEE*, Ahmed Bader, *Senior Member, IEEE*, and Mohamed-Slim Alouini, *Fellow, IEEE*

***Abstract*— One of the main challenges slowing the deployment of airborne base stations (BSs) using unmanned aerial vehicles (UAVs) is the limited on-board energy and flight time. One potential solution to such problem, is to provide the UAV with power supply through a tether that connects the UAV to the ground. In this paper, we study the optimal placement of tethered UAVs (TUAVs) to minimize the average path-loss between the TUAV and a receiver located on the ground. Given that the tether has a maximum length, and the launching point of the TUAV (the starting point of the tether) is placed on a rooftop, the TUAV is only allowed to hover within a specific *hovering region*. Beside the maximum tether length, this hovering region also depends on the heights of the buildings surrounding the rooftop, which requires the inclination angle of the tether not to be below a given minimum value, in order to avoid tangling and ensure safety. We first formulate the optimization problem for such setup and provide some useful insights on its solution. Next, we derive upper and lower bounds for the optimal values of the tether length and inclination angle. We also propose a suboptimal closed-form solution for the tether length and its inclination angle that is based on maximizing the line-of-sight probability. Finally, we derive the probability distribution of the minimum inclination angle of the tether length. We show that its mean value varies depending on the environment from $10^\circ$ in suburban environments to $31^\circ$ in high rise urban environments. Our numerical results show that the derived upper and lower bounds on the optimal values of the tether length and inclination angle lead to tight suboptimal values of the average path-loss that are only $0-3$ dBs above the minimum value.**

***Index Terms*— Unmanned aerial vehicles, tethered drones, cellular networks, optimal placement.**

## I. Introduction

With the increasing number of use cases and applications of unmanned aerial vehicles (UAVs) in the past few years [1]–[5], developing communication systems tailored to serve such high altitude nodes was inevitable. This is evident by the existence of UAV-related work items in recent releases of 3GPP [6]. As a result of relying on the cellular network to provide the communication support for those airborne users, many research works were motivated to study the fundamental differences between serving terrestrial and aerial users, main challenges, and possible solutions [7]–[13].

The research in that area has later evolved to studying the potential of using UAVs as flying base stations (BSs) to serve terrestrial users [14]–[18]. This is motivated by the improved channel quality between the BS and the user when the BS is deployed at high altitude, due to the high probability of establishing a line-of-sight (LoS) channel. In addition, the mobility and relocation capability of the envisioned UAV-mounted BS would highly increase the flexibility of its deployment, which is perfect in areas with time-varying traffic demand spatial distribution [19]. Furthermore, due to its easy and quick deployment (plug and play), UAV can be used for emergency scenarios and disaster recovery to serve mobile users in recovering areas [20]. Existing literature has considered multiple aspects of the flying BS system, such as mobility modeling [21], [22], trajectory optimization [23]–[27], optimal deployment for limited hovering time [28], interference analysis [29], and coexistence with device-to-device (D2D) networks [30].

Unfortunately, as promising as flying BSs might seem, practical limitations prevented it from attracting similar attention from the industrial sector, with some exceptions that will be discussed later in this section. These limitations include: (i) achievable UAV payload, (ii) flight time, and (iii) on-board available energy for processing and communication.

*Achievable Payload:* In order to use the UAV as a flying BS, we need to equip it with antennas and multiple processing units. However, achievable payloads for currently available UAVs are very limited. This, in turns, disables some important features such as sectorization and antenna diversity. In order to increase the payload of a UAV, we need to provide it with a stable source of energy, which is not available in untethered UAVs. This results from the fact that the UAV's power consumption is an increasing function of the weight of the UAV and its payload, as discussed in detail in [31], [32].

*Flight Time:* The limited flight time of the UAV is one of the main obstacles in the road towards realizing UAV-mounted BSs. The current state of the art can only achieve less than an hour of hovering time before battery depletion. Hence, the UAV needs to revisit a ground station every hour to recharge or change the battery and then fly back to its hovering location. This leaves the UAV coverage area temporarily out of service, which reduces the performance of the cellular network.

Manuscript received October 20, 2019; revised March 11, 2020 and May 3, 2020; accepted May 4, 2020. Date of publication May 11, 2020; date of current version August 14, 2020. This work was funded in part by the Center of Excellence for NEOM Research at KAUST. The associate editor coordinating the review of this article and approving it for publication was Y. Liu. *(Corresponding author: Mustafa A. Kishk.)*

Mustafa A. Kishk and Mohamed-Slim Alouini are with the CEMSE Division, King Abdullah University of Science and Technology (KAUST), Thuwal 23955-6900, Saudi Arabia (e-mail: mustafa.kishk@kaust.edu.sa; slim.alouini@kaust.edu.sa).

Ahmed Bader is with Insyab Wireless Ltd., Dubai 1961, United Arab Emirates (e-mail: ahmed@insyab.com).

Color versions of one or more of the figures in this article are available online at http://ieeexplore.ieee.org.

Digital Object Identifier 10.1109/TCOMM.2020.2993885

TABLE I
TUAV STATE OF THE ART

| Company name | Maximum tether length | Flight time |
|---|---|---|
| Equinox Systems [42] | 150 m | 30 Days |
| TDS [43] | 120 m | unlimited |
| Aria Insights [44] | 120 m | multi-day operation |
| Elistair [45] | 80 m | 10+ hours |

*On-Board Available Energy:* A cellular BS is one of the most power consuming components of the cellular network. It requires power for data transmission, processing, and backhauling. While 4G cell-sites consume around 6 kilowatts, 5G cell-sites are expected to consume around 10-15 kilowatts [33]. With the available limited battery on-board in current UAVs, providing the required power for communication and processing is a challenge.

Looking back at the above three main practical limitations, we observe that the key solution to achieve a reliable, stable, and sustainable flying BS is ensuring a stable source of energy for the UAV [34], [35]. Fortunately, this is provided in *tethered UAVs* (TUAVs) [36]. With a stable power supply provided to the UAV through a tether connected to the ground station (GS), the TUAV can achieve much longer flight times, support heavier payload, and support the required power for on-board communication and processing. In addition to providing the TUAV with power supply, a wired data link is also extended through the tether. This enables a wired backhaul link between the flying BS and the GS, which solves another significant challenge in untethered UAV-mounted BSs, namely, wireless backhaul communication [37]–[40]. The tether acts as a medium that carries two cables: (i) power carrying cable, and (ii) data carrying cable. One end of each of these cables is connected to the UAV and the other end is connected to the GS. Due to its great potential to realize a flying BS, many companies around the world have started developing TUAVs, which are actually available for commercial use. In Table I, we summarize the specifications of TUAVs implemented by these companies.

Recently, TUAVs were used by an American service provider in Puerto Rico to provide cellular coverage for the recovering areas after the hurricane Maria [41]. In fact, the majority of the companies mentioned in Table I rely on a specific set of applications for promoting their TUAV products such as surveillance, broadcasting, video streaming for assessment of critical situations, search and rescue, and providing cellular coverage for emergency scenarios until the damaged cell towers are rebuilt. However, the recent technological advances and the current achievable specifications, see [42] for example, make TUAVs a very attractive solution for non-emergency related scenarios such as offloading terrestrial BSs in locations with high traffic demand, providing cellular coverage in remote and rural areas, and network densification [36].

*TUAVs vs. Helikites:* Note that TUAVs are different from, the more famous, *Helikites* in multiple aspects. Helikites were recently adopted for deploying flying BSs at high altitudes [38]. Helikites are designed in a way that combines some properties of kites and helium balloons. Thanks to the intelligent aerodynamic design of Helikites, they do not need to be power supplied in order to stay in the air. However, they are connected to the ground through a tether, which restrains the Helikite and prevents it from floating away. Just like TUAVs, Helikites are capable of supporting relatively large payloads. However, there are some specific operation conditions that need to be satisfied to support such large payloads. For instance, a 15 $m^3$ Helikite needs at least 15 miles/hour wind speed to be able to support a payload of 12 Kgs [46]. This operation conditions are relaxed when the size of the Helikite is increased. If the Helikite size is increased to 34 $m^3$, it is able to support a payload of upto 14 Kgs without the need to any wind. For heavier payloads, higher speed wind is required. Such wind speeds might not be available at lower altitudes, which means that successful operation requires either high altitude deployment or increasing the Helikite sizes [46]. On the other hand, TUAVs are much lower in size (less than 3 $m^3$ [42]), but their reachable altitude is restricted by the tether length. Another concern that comes to picture when using Helikites for providing cellular coverage, is the energy requirements of its payload. Beside antennas, the Helikite also carries processing units on-board, which need to be powered. Given that the Helikite's tether does not provide it with power supply, the only option to power the on-board payload is carrying a battery on the Helikite, which limits the endurance of the flying BS [46]. We can conclude from this discussion that there is a fundamental difference between TUAVs and Helikites in terms of architecture, achievable altitudes, payloads, design challenges, and operating conditions. Hence, we believe that the use cases and applications that would benefit from TUAVs and Helikites are quite different, which means that the two technologies are complementary to each other with similar importance for future wireless networks.

*TUAVs vs. Untethered UAVs:* In order to consider widely deploying TUAVs for cellular coverage enhancement, performance of such setup should be carefully studied first. In particular, analysis of such systems should be performed while taking into account the special characteristics of the TUAV such as the limited tether length and the safety considerations to avoid tangling the tether upon surrounding buildings. These characteristics lead to a set of problems that are fundamentally different from the problems typically considered in the literature of untethered UAVs. In this paper, we focus on one particular problem related to the 3D placement of TUAV in a point-to-point system. Assuming one user at a distance $d$ from the rooftop, at which the GS is deployed, we aim to find the optimal location of the TUAV that minimizes the average path-loss. For an untethered UAV, this problem would have a trivial solution of placing the UAV right above the user, exploiting the mobility freedom available in untethered UAVs [22], [47]. However, for a TUAV, the placement problem is more constrained, due to the restricted tether length and inclination angle. We analyze this setup and provide a mathematical framework that captures the special properties of TUAVs. More details on the contributions of this paper will be in Sec. I-B.

### A. Related Work

TUAVs' share of the existing literature is very limited. The only works that shed some light on such setup are [48], [49]. In [48], the authors proposed using TUAVs in post-disaster scenarios, due to the existence of a wired data link through the tether, to provide a backhaul link for the untethered UAVs. In particular, while the untethered drones are dedicated to providing cellular coverage for the recovering area, they use a free-space-optical (FSO) link with the TUAV for backhaul. In [49], the authors studied the optimal trajectory of an untethered UAV serving two users, which are apart with distance $D$. However, when the product of the distance and the velocity of the UAV is much lower than the flight time of the UAV, the problem considered in this paper reduces to finding the optimal hovering location, instead of the optimal trajectory. This can be considered equivalent to the deployment problem of a TUAV, if the TUAV is always located exactly above its GS, with the tether length extended to its maximum value. However, this assumption might not hold in many scenarios. For instance, one of these scenarios is when it is not possible to place the GS at the projection of the optimal TUAV location. In that case, the selection of the GS location, as well as the TUAV placement should be optimized. We aim in this paper to capture the main differences between the placement problem of tethered and untethered UAVs. Our main objective is to study how the tether length and inclination angle should be tuned to optimize the TUAV location.

The existing works in literature that worked on UAV placement and trajectory optimization problems focused solely on untethered UAVs. One of the most important works in that direction was provided in [50]. In this paper, the authors focused on optimizing the altitude of the UAV to maximize its coverage radius. In particular, they provided an expression for the average path-loss expression as a function of the altitude and the distance between the UAV's projection and the receiver. Using that expression, the radius of the area where the receivers obtain an average path-loss below a predefined threshold is maximized. Authors in [51], considered similar setup with the objective of minimizing the transmit power of the UAV. In [52], the authors tackled the optimal placement problem with the objective of minimizing the number of required UAVs. In [53], the authors considered a system of multi-antenna UAVs used to provide coverage for a given area. The coverage probability, defined as the probability that the signal-to-interference-plus-noise-ratio (SINR) is above a predefined threshold, is derived. The altitudes of the UAVs is then optimized to maximize the coverage probability using circle packing theory. In [54], the UAV optimal placement problem was considered with the objective of maximizing the number of covered users, where a user is covered if its perceived path-loss is below a specific value. The results showed that the UAV deployment is efficient, in terms of average number of covered users, in suburban and urban regions. However, the mean number of covered users decreases dramatically in high rise urban regions. In [55], a system of UAVs is used to collect data from an Internet of Things (IoT) network. For that setup, the authors optimize the deployment of the UAVs as well as their mobility from one location to another, based on the activity of the IoT devices. Reducing the mobility of the UAVs as much as possible is of great importance for untethered UAVs, because it consumes most of the available energy on-board. This concern, however, does not come to picture when TUAVs are deployed, due to the existence of a stable power supply through the tether.

Another important part of literature that focused on the performance evaluation of UAV-assisted communication is stochastic geometry-based literature [14], [18], [20], [21], [29], [40], [47], [56]–[59]. Random process theory has been used in literature to model the locations of the UAVs and the users in order to study the performance of UAV-assisted networks in multiple scenarios such as post-disaster communication networks [20], finite networks [29], 3GPP-inspired models [47], UAV deployment above hotspots [57], and UAV-assisted millimeter wave networks [58].

It can be observed from the above discussion that the main design parameters of an untethered UAV-enabled communication system are (i) the UAV's altitude, (ii) the location of its projection on the ground, and (iii) its trajectory. These parameters are typically optimized to maximize the coverage of the UAV and minimize its energy consumption, in order to increase the flight time. On the other hand, a TUAV does not have concerns related to mobility minimization, as stated, due to the existence of a stable source of energy through the tether. However, unlike untethered UAVs, the altitude and projection of the TUAV are constrained with the maximum tether length. Hence, compared to untethered UAVs, the optimal placement problem of a TUAV has some fundamental differences, which is what we aim to study in this paper. The contributions of this paper are summarized next.

### B. Contributions

Compared to the existing literature on placement optimization of UAV-mounted BSs, which solely focused on untethered UAVs, this paper's main objective is to optimize the location of a tethered UAV (TUAV) using its tether length and inclination angle as the main optimization parameters. We consider a TUAV system where the GS (the starting point of the tether) is placed on the rooftop of a building and a receiver located at a given distance from the building. Aligning with available TUAV state of the art, we assume that the tether has a maximum length, which limits its mobility and relocation capability. In addition, motivated by the importance of the tether for supporting the TUAV with both power and data, we assume that the inclination angle of the tether can not be below a specific value. This value ensures that the tether will not get tangled upon any of the surrounding builds.

*1) A Novel Mathematical Framework for Modeling and Analysis of TUAVs:* We provide a mathematical model for the achievable locations by the TUAV in the 3-dimensional (3-D) plane, which we refer to as the *hovering region*. Next, we formalize the optimal placement problem that aims to minimize the average path-loss at the receiver, with the hovering region as the main constraint of the optimization problem. Before solving the problem, we carefully analyze it and provide multiple insights on its solution. The proposed mathematical

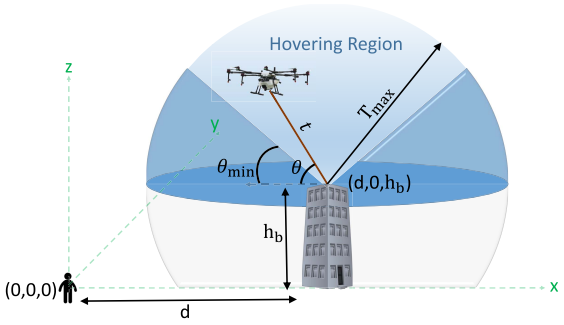


Fig. 1. The system setup considered in this paper.

framework captures the main differences in the analysis of tethered and untethered UAVs. In particular, it captures the effect of the tether length and minimum inclination angle on the performance of the system.

*2) Upper and Lower Bounds for the Optimal Values of the Tether Length and Inclination Angle:* Using the drawn insights on the placement problem, we derive upper and lower bounds for the optimal values of the optimal tether length and inclination angle. In particular, when the distance between the receiver and the building is below a certain threshold, we show that the optimal value of the inclination angle is its minimum value and provide upper and lower bounds for the tether length. When the distance is above the threshold, we show that the optimal tether length is its maximum value and derive upper and lower bounds for the optimal inclination angle. We show using numerical results, assuming a dense urban environment, that the upper and lower bounds lead to tight results with respect to the optimal average path-loss value.

*3) Closed-Form Expressions for Suboptimal Solution:* We propose a suboptimal solution for the TUAV placement problem that is based on maximizing the probability of LoS. We derive closed form expressions for the suboptimal values of the tether length, inclination angle, and average path-loss. We evaluate the tightness of this suboptimal solution in a dense urban environment using numerical results. The results show that the suboptimal value of the average path-loss is only $0-3$ dBs above the optimal value.

*4) Probability Distribution of the Minimum Inclination Angle in Different Environments:* As stated earlier, the minimum allowed value for the inclination angle is based on the altitude of the rooftop with respect to its surrounding buildings. The inclination angle should be high enough to prevent tangling. Based on that approach, we use tools from stochastic geometry to model the locations of the buildings and concretely derive the probability distribution of the inclination angle minimum value. We show that the inclination angle's mean value varies from $10^\circ$ at suburban environments to $31^\circ$ at high rise urban regions.

## II. System Setup

As shown in Fig. 1, we consider a system composed of a TUAV launched from a GS that is placed on a rooftop at height $h_b$. The TUAV has the freedom to hover anywhere within the hemisphere centered at the rooftop with radius equal to the maximum value of the tether length $T_{\max}$. In order to avoid tangling upon surrounding buildings and ensure safety of the tether, the inclination angle $\theta$ of the tether, has a minimum value $\theta_{\min}$, as shown in Fig. 1. We use Cartesian coordinates $(x, y, z)$ in the rest of the paper, to represent the locations of the TUAV and the receiver. Without loss of generality, we assume that the receiver is located at the origin $(0, 0, 0)$, while the rooftop is located at the point $(d, 0, h_b)$, where $d$ is the distance between the receiver and the building. Based on values of $\theta_{\min}$, $h_b$, and $T_{\max}$, the TUAV can be deployed anywhere within a specific *hovering region*, which is defined next.

*Definition 1: The hovering region of the TUAV, is the set of locations in $\mathbb{R}^3$ that are reachable by the TUAV:*

$$\mathcal{M} = \Bigg\{ p \in \mathbb{R}^3 : \sqrt{(x_p - d)^2 + (y_p)^2 + (z_p - h_b)^2} \leq T_{\max}, \sin^{-1}\left( \frac{z_p - h_b}{\sqrt{(x_p - d)^2 + (y_p)^2 + (z_p - h_b)^2}} \right) \geq \theta_{\min} \Bigg\}, \quad (1)$$

*where $(x_p, y_p, z_p)$ are the Cartesian coordinates of the point $p$.*

The TUAV aims to find the location within the hovering region that has the minimum average path-loss (PL), which is defined next.

*Definition 2: The average PL between a TUAV located at $p$ and the receiver is [50]:*

$$\mathrm{PL_p} = \left( \frac{4\pi}{\lambda} \right)^2 \left( P_{\mathrm{LoS}}(p) R_p^2 \eta_{\mathrm{LoS}} + (1 - P_{\mathrm{LoS}}(p)) R_p^2 \eta_{\mathrm{nLoS}} \right), \quad (2)$$

*where $\lambda$ is the signal wavelength, $P_{\mathrm{LoS}}$ is the line-of-sight (LoS) probability, $R_p = \sqrt{x_p^2 + y_p^2 + z_p^2}$ is the distance between the receiver and the TUAV, and $\eta_{\mathrm{LoS}} < \eta_{\mathrm{nLoS}}$ are the mean excessive path-loss values for the cases of LoS and non-LoS, respectively.*

Next, we formally define the LoS probability, which highly impacts the value of PL, and, in turns, the optimal placement problem.

*Definition 3: The LoS probability between a TUAV located at $p$ and the receiver, provided in [60], is*

$$P_{\mathrm{LoS}}(p) = a \left( \tan^{-1}\left( \frac{z_p}{\sqrt{x_p^2 + y_p^2}} \right) - 15 \right)^b, \quad (3)$$

*where the values of the parameters $a$ and $b$ depend on whether the environment is suburban, urban, dense urban, or high rise urban.*

The ultimate goal of TUAV placement is to find the location, within its hovering region, that minimizes the average PL between the TUAV and the receiver. The optimization problem

can be formally written as follows.

$$\mathbf{OP_1}: \underset{p\in\mathbb{R}^3}{\text{minimize}} \quad \mathrm{PL}_p$$
$$\text{subject to: } t_p = \sqrt{(x_p-d)^2+(y_p)^2+(z_p-h_b)^2} \leq T_{\max}, \tag{4a}$$
$$\theta_p = \sin^{-1}\left(\frac{z_p-h_b}{\sqrt{(x_p-d)^2+(y_p)^2+(z_p-h_b)^2}}\right) \geq \theta_{\min}, \tag{4b}$$

where $t_p$ is the length of the tether required to locate the TUAV at $p \in \mathbb{R}^3$, $\theta_p$ is the inclination angle between the tether and the tether and the $x-y$ plane, constraint (4a) ensures that the tether length is below its maximum value and constraint (4b) ensures that the tether inclincation angle is above its minimum value. These constraints represent the main difference between the placement problem of a TUAV and an untethered UAV. Even with a restriction on the altitude of the untethered UAV, the only constraint would be $z_p \leq z_{\max}$, which is clearly different from the constraints in $\mathbf{OP_1}$.

*Proposition 1: For any two points $p_1, p_2 \in \mathbb{R}^3$, if $z_{p_1} = z_{p_2}$ and $R_{p_1} < R_{p_2}$, then $\mathrm{PL}_{p_1} < \mathrm{PL}_{p_2}$. Proof: Given that $z_{p_1} = z_{p_2}$ and $R_{p_1} < R_{p_2}$, we know that $\sqrt{x_{p_1}^2+y_{p_1}^2} < \sqrt{x_{p_2}^2+y_{p_2}^2}$. Revisiting (3), we conclude that $P_{\mathrm{LoS}}(p_1) > P_{\mathrm{LoS}}(p_2)$. Given that $\eta_{\mathrm{LoS}} < \eta_{\mathrm{nLoS}}$, the statement in the proposition follows.* ■

*Proposition 2: The optimal location for the TUAV, $p_{\mathrm{opt}}$, satisfies the following*:

$$y_{p_{\mathrm{opt}}} = 0. \tag{5}$$

*Proof: For any point, p, with $|y_p| > 0$, that satisfies (4a) and (4b), its projection on the x-z plane $\{y = 0\}$, $\hat{p}$, has the following characteristics*:

$$z_{\hat{p}} \overset{(a)}{=} z_p, \quad x_{\hat{p}} = x_p, \quad y_{\hat{p}} = 0.$$

*Hence, given that $|y_{\hat{p}}| < |y_p|$, we can conclude that $R_{\hat{p}} \overset{(b)}{<} R_p$. Now given that p satisfies constraints (4a) and (4b), then $\hat{p}$ also satisfies constraints (4a) and (4b). Also, based on (a), and (b), and using Proposition 1, we conclude that $\mathrm{PL}_{\hat{p}} < \mathrm{PL}_p$.* ■

*Proposition 3: The optimal location for the TUAV, $p_{\mathrm{opt}}$, satisfies the following*:

$$0 < x_{p_{\mathrm{opt}}} < d. \tag{6}$$

*Proof: We first prove that $x_{p_{\mathrm{opt}}} < d$ as follows. For any point, p, with $x_p > d$, that satisfies (4a) and (4b), consider a point $\hat{p}$ with the following characteristics*:

$$z_{\hat{p}}=z_p, \quad x_{\hat{p}} = 2d - x_p, \quad y_{\hat{p}} = y_p. \tag{7}$$

*Hence, given that $(x_{\hat{p}}-d)^2 = (x_p-d)^2$, then $\hat{p}$ also satisfies constraints (4a) and (4b). In addition, since $x_p > d$, then $x_{\hat{p}}^2 < x_p^2$. Hence, $R_{\hat{p}} < R_p$ and $P_{\mathrm{LoS}}(\hat{p}) > P_{\mathrm{LoS}}(p)$, which implies that $\mathrm{PL}_{\hat{p}} < \mathrm{PL}_p$.*

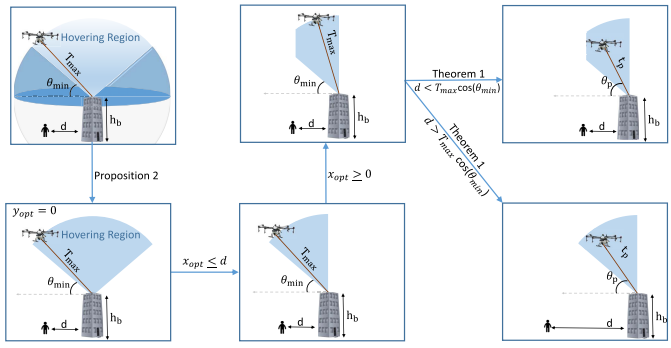


Fig. 2. The effect of Propositions 2 and 3 on the hovering region.

*Now we prove that $x_{p_{\mathrm{opt}}} > 0$ as follows. For any point, p, with $x_p < 0$, that satisfies (4a) and (4b), consider a point $\hat{p}$ with the following characteristics*:

$$z_{\hat{p}}=z_p, \quad x_{\hat{p}} = 0, \; y_{\hat{p}} = y_p. \tag{8}$$

*Hence, given that $x_p < 0$, then $(x_{\hat{p}}-d)^2 < (x_p-d)^2$, which ensures that $\hat{p}$ also satisfies constraints (4a) and (4b). Also, since $x_{\hat{p}}^2 < x_p^2$, we conclude that $R_{\hat{p}} < R_p$ and $P_{\mathrm{LoS}}(\hat{p}) > P_{\mathrm{LoS}}(p)$, which implies that $\mathrm{PL}_{\hat{p}} < \mathrm{PL}_p$.* ■

Given that $t$ is the length of tether and $\theta$ is the angle between the tether and the $x-y$ plane, we can use the above propositions and the fact that $x = d - t\cos(\theta)$ and $z = h_b + t\sin(\theta)$ to rewrite the optimization problem $\mathbf{OP_1}$ in terms of $t$ and $\theta$ instead of $x$, $y$, and $z$. The equivalent optimization problem is provided next.

$$\mathbf{OP_2}: \underset{t_p,\theta_p}{\text{minimize}} \quad \mathrm{PL}_p$$
$$\text{subject to: } \theta_{\min} \leq \theta_p \leq \frac{\pi}{2}, \tag{9a}$$
$$t_p\cos(\theta_p) \leq d, \tag{9b}$$
$$0 \leq t_p \leq T_{\max}, \tag{9c}$$

where constraints (9a) and (9b) ensure that $0 < x < d$ as discussed in Proposition 3, and constraint (9c) ensures that the tether length is less than its maximum value.

*Remark 1: It can be observed from $\mathbf{OP_2}$ that having $d > T_{\max}\cos(\theta_{\min})$ implies that $d > t_p\cos(\theta_p)$ for all $t_p < T_{\max}$ and $\theta_{\min} \leq \theta_p \leq \frac{\pi}{2}$. In other words, if $d > T_{\max}\cos(\theta_{\min})$, constraint (9b) is always satisfied. This case is shown in Fig. 2 for more clarification.*

## III. Optimal and Suboptimal Solutions

### A. Upper and Lower Bounds on the Optimal Solution

In this section, we aim to study the optimization problem $\mathbf{OP_2}$ and provide upper and lower bounds for the optimal values of the tether length $t_p$ and the inclination angle $\theta_p$. In the following theorem, we show that the optimal location of the TUAV lies on the border of the hovering region, between the rooftop and the receiver, as shown in Fig. 3.

*Theorem 1: When $d > T_{\max}\cos(\theta_{\min})$, the optimal values of $(t_p, \theta_p)$ belong to the following set*

$$\mathcal{H} = \mathcal{H}_1 \cup \mathcal{H}_2, \tag{10}$$

TABLE II
TABLE OF NOTATIONS

| Notation | Description |
|---|---|
| $\mathrm{PL}_p$ | The average path-loss between a TUAV located at $p \in \mathbb{R}^3$ and the receiver located at the origin |
| $R_p$ | The distance between a TUAV located at $p \in \mathbb{R}^3$ and the receiver |
| $P_{\mathrm{LoS}}(p)$ | The LoS probability between a TUAV located at $p \in \mathbb{R}^3$ and the receiver |
| $t_p$ | The length of the tether when the TUAV is placed at $p \in \mathbb{R}^3$ |
| $\theta_p$ | The inclination angle of the tether with respect to the x-y plane when the TUAV is placed at $p \in \mathbb{R}^3$ |
| $\theta_{\min}$ | The minimum allowed inclination angle, to avoid tangling with surrounding buildings |
| $\eta_{\mathrm{LoS}}$; $\eta_{\mathrm{nLoS}}$ | the mean value of the excessive path-loss for the cases of LoS and non-LoS, respectively |
| $t_{\mathrm{opt}}$; $t_{\mathrm{sub}}$ | Optimal; suboptimal values of the tether length |
| $\theta_{\mathrm{opt}}$; $\theta_{\mathrm{sub}}$ | Optimal; suboptimal values of the tether inclination angle |

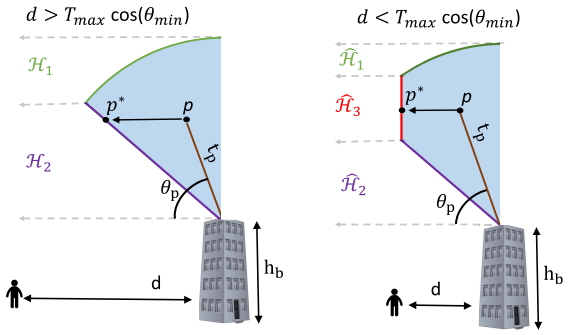


Fig. 3. As explained in Theorem 1, $\mathrm{PL}_p$ is always greater than $\mathrm{PL}_{p^*}$.

*where*

$$\mathcal{H}_1 = \left\{(t,\theta) : \theta_{\min} \le \theta \le \frac{\pi}{2}, t = T_{\max}\right\}, \tag{11}$$

*and*

$$\mathcal{H}_2 = \left\{(t,\theta) : \theta = \theta_{\min}, 0 < t < T_{\max}\right\}. \tag{12}$$

*When* $d < T_{\max}\cos(\theta_{\min})$, *the optimal values of* $(t_p, \theta_p)$ *belong to the following set*

$$\hat{\mathcal{H}} = \hat{\mathcal{H}}_1 \cup \hat{\mathcal{H}}_2 \cup \hat{\mathcal{H}}_3, \tag{13}$$

*where*

$$\hat{\mathcal{H}}_1 = \left\{(t,\theta) : \cos^{-1}\left(\frac{d}{T_{\max}}\right) \le \theta \le \frac{\pi}{2}, t = T_{\max}\right\}, \tag{14}$$

$$\hat{\mathcal{H}}_2 = \left\{(t,\theta) : \theta = \theta_{\min}, 0 < t \le \frac{d}{\cos(\theta_{\min})}\right\}, \tag{15}$$

$$\hat{\mathcal{H}}_3 = \left\{(t,\theta) : \theta_{\min} \le \theta \le \cos^{-1}\left(\frac{d}{T_{\max}}\right), t = \frac{d}{\cos(\theta)}\right\}. \tag{16}$$

*Proof: To avoid repetition, we will focus in the proof on the case of* $d > T_{\max}\cos(\theta_{\min})$. *Recalling that for any point p, satisfying the three constraints in* $\mathbf{OP_2}$, *we know that* $z_p = h_b + t_p\sin(\theta_p)$ *and* $x_p = h_b - t_p\cos(\theta_p)$. *Now, as shown in Fig. 3, for any point* $p \notin \mathcal{H}$, *its projection* $p^*$ *on* $\mathcal{H}$ *has the following characteristics:*

$$z_{p^*} = \begin{cases} h_b + T_{\max}\sin(\theta_{p^*}) & \text{if } p^* \in \mathcal{H}_1 \\ h_b + t_{p^*}\sin(\theta_{\min}) & \text{if } p^* \in \mathcal{H}_2. \end{cases} \tag{17}$$

*Given that* $z_{p^*} = z_p$, $\theta_p > \theta_{\min}$, *and* $t_p < T_{\max}$, *then we can conclude that* $\theta_{p^*} < \theta_p$ *and* $t_p < t_{p^*}$. *Hence, it can be easily shown that* $x_p > x_{p^*}$, *which means that* $R_p > R_{p^*}$. *Using Proposition 1, we can show that* $\mathrm{PL}_p > \mathrm{PL}_{p^*}$, *which concludes the proof.* ■

*Corollary 1: For the case of* $d < T_{\max}\cos(\theta_{\min})$, *the optimal values of* $(t_p, \theta_p)$ *belong to* $\hat{\mathcal{H}}_2 = \{(t,\theta) : \theta = \theta_{\min}, 0 < t \le \frac{d}{\cos(\theta_{\min})}\}$. *Proof: The point* $p = \left(t_p = \frac{d}{\cos(\theta_{\min})}, \theta_p = \theta_{\min}\right) \in \hat{\mathcal{H}}_2$ *has an elevation angle* $\tan^{-1}\left(\frac{z_p}{\sqrt{y_p^2+x_p^2}}\right) = \tan^{-1}\left(\frac{h_b+t_p\sin(\theta_p)}{d-t_p\cos(\theta_p)}\right) = \frac{\pi}{2}$ *and* $R_p = h_b + d\tan(\theta_{\min})$. *Hence, recalling (3), for any point* $p^* \in \hat{\mathcal{H}}_1 \cup \hat{\mathcal{H}}_3$, *we have* $P_{\mathrm{LoS}}(p) \ge P_{\mathrm{LoS}}(p^*)$ *and* $R_p < R_{p^*}$, *which means that* $\mathrm{PL}_p < \mathrm{PL}_{p^*}$. ■

*Remark 2: By observing Fig. 3, we can interpret Theorem 1 and Corollary 1 as follows. Recalling (2), the average path-loss* $\mathrm{PL}_{\mathrm{p}}$ *is a decreasing function of* $P_{\mathrm{LoS}}(p)$ *and an increasing function of the distance* $R_p = \sqrt{x_p^2 + y_p^2 + z_p^2}$. *Also, recalling (3),* $P_{\mathrm{LoS}}(p)$ *is an increasing function of the elevation angle* $\theta_e(p) = \tan^{-1}\frac{z_p}{\sqrt{x_p^2+y_p^2}}$. *The results in Theorem 1 and Corollary 1 imply that the optimal point for a given elevation angle* $\theta_e$ *is simply the closest point in the hovering region* $\mathcal{M}$ *that achieves this elevation angle. For that reason, the optimal point belongs to the boundaries of the hovering region as shown in Fig. 3.*

Now, in the following two lemmas, we provide some important insights on $R_p$ and $P_{\mathrm{LoS}}(p)$ that will be useful for defining upper and lower bounds on the optimal values of $t_p$ and $\theta_p$.

*Lemma 1: For any given* $\theta_p$, *where* $\theta_{\min} < \theta_p < \frac{\pi}{2}$, $R_p$ *is a convex function of* $t_p$ *where* $\arg\min_{t_p} R_p = t^*(\theta_p) = d\cos(\theta_p) - h_b\sin(\theta_p)$. *In addition,* $P_{\mathrm{LoS}}(p)$ *is an increasing function of* $t_p$.

*Proof: See Appendix A.* ■

*Lemma 2: For any given $t_p$, where $0 < t_p \leq T_{\max}$, $R_p$ is an increasing function of $\theta_p$ in the set $\mathcal{S} = \{\theta_{\min} < \theta_p < \frac{\pi}{2}\}$. In addition, $P_{\mathrm{LoS}}(p)$ is a concave function of $\theta_p$ in the set $\mathcal{S}$, where*

$$\arg\max_{\theta_p} P_{\mathrm{LoS}}(p) = \theta^*(t_p) = \sin^{-1}\left(\frac{d}{\sqrt{d^2+h_b^2}}\right) - \sin^{-1}\left(\frac{t_p}{\sqrt{d^2+h_b^2}}\right). \quad (18)$$

*Proof: See Appendix B.* ∎

In the following theorem, we provide upper and lower bounds for the optimal values of $t$ and $\theta$ for different values of $d$.

*Theorem 2: The solution to $\mathbf{OP_2}$ is $(t_p, \theta_p) \in \mathcal{H}_{\mathrm{opt}}$, where*

$$\mathcal{H}_{\mathrm{opt}} = \begin{cases} \underbrace{\left\{(t_{\mathrm{opt}}, \theta_{\min}) : \ \max(0, t^*(\theta_{\min})) \leq t_{\mathrm{opt}} \leq \frac{d}{\cos(\theta_{\min})}\right\}}_{\text{if } d \leq T_{\max}\cos(\theta_{\min})}, \\ \underbrace{\{(t_{\mathrm{opt}}, \theta_{\min}) : \ \max(0, t^*(\theta_{\min})) \leq t_{\mathrm{opt}} \leq T_{\max}\}}_{\text{if } T_{\max}\cos(\theta_{\min}) \leq d \leq \mathcal{F}}, \\ \underbrace{\{(T_{\max}, \theta_{\mathrm{opt}}) : \ \theta_{\min} \leq \theta_{\mathrm{opt}} \leq \theta^*(T_{\max})\}}_{\text{if } d \geq \mathcal{F}}, \end{cases} \quad (19)$$

*$\max(k, m)$ is the maximum value between $k$ and $m$, $\mathcal{F} = \frac{T_{\max}}{\cos(\theta_{\min})} + h_b \tan(\theta_{\min})$, $t^*(\theta_{\min}) = d\cos(\theta_{\min}) - h_b \sin(\theta_{\min})$, and $\theta^*(T_{\max}) = \sin^{-1}\left(\frac{d}{\sqrt{d^2+h_b^2}}\right) - \sin^{-1}\left(\frac{T_{\max}}{\sqrt{d^2+h_b^2}}\right)$.*

*Proof: We start with the case of $d \leq T_{\max}\cos(\theta_{\min})$. In that case, as shown in Corollary 1, the optimal value of $\theta$ is $\theta_{\min}$, and the optimal value of $t$ falls in the range $0 < t \leq \frac{d}{\cos(\theta_{\min})}$. Recalling Lemma 1, and given that $PL_p$ is a decreasing function of $P_{\mathrm{LoS}}(p)$ and an increasing function of $R_p$, we can easily conclude that $t^*(\theta_{\min}) \leq t_{\mathrm{opt}}$.*

*For the case of $T_{\max}\cos(\theta_{\min}) \leq d \leq \mathcal{F}$, it can easily be shown that $t^*(\theta_{\min}) < T_{\max}$ and $\theta^*(T_{\max}) < \theta_{\min}$. Hence, recalling Theorem 1, we can show that $(\theta_{\min}, T_{\max})$ is the optimal point in $\mathcal{H}_1$ by using Lemma 2. Similarly, revisiting $\mathcal{H}_2$ in Theorem 1, we can also show that $t_{\mathrm{opt}} \geq t^*(\theta_{\min})$, using Lemma 1.*

*For the case of $d \geq \mathcal{F}$, it can be shown that $t^*(\theta_{\min}) > T_{\max}$ and $\theta^*(T_{\max}) > \theta_{\min}$. Hence, we can show that $(\theta_{\min}, T_{\max})$ is the optimal point in $\mathcal{H}_2$ by using Lemma 1. In addition, we can use Lemma 2 to show that $\theta_{\mathrm{opt}} \leq \theta^*(T_{\max})$. This concludes the proof.* ∎

*Remark 3: After establishing in Remark 2 that the optimal point belongs to the boundaries of the hovering region $\mathcal{M}$. In Theorem 2 we show that optimal point lies between two locations in $\mathcal{M}$: (i) the closest point to the receiver, and (ii) the point that has the largest elevation angle.*

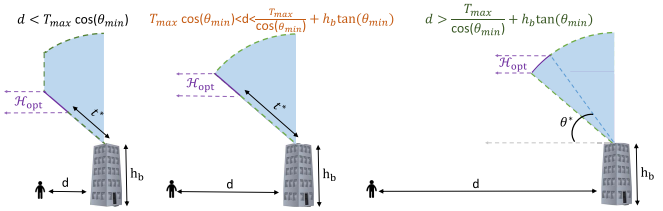


Fig. 4. The regions we should search for the optimal location of the TUAV $\mathcal{H}_{\mathrm{opt}}$, for different values of $d$.

*For each of the three scenarios in Fig. 4, the closest points are $\{t^*, \theta_{\min}\}$, $\{t^*, \theta_{\min}\}$, and $\{T_{\max}, \theta_{\min}\}$, while the points with the largest elevation angles are $\{\frac{d}{\cos(\theta_{\min})}, \theta_{\min}\}$, $\{T_{\max}, \theta_{\min}\}$, and $\{T_{\max}, \theta^*\}$, respectively.*

*Corollary 2: For the case of $\theta_{\min} = 0°$, the results in Theorem 2 reduce to*

$$(t_{\mathrm{opt}}, \theta_{\mathrm{opt}}) = \begin{cases} \underbrace{(d, 0°)}_{\text{if } d \leq T_{\max}}, \\ \underbrace{(T_{\max}, \theta_{\mathrm{opt}}), \ 0° \leq \theta_{\mathrm{opt}} \leq \theta^*(T_{\max}).}_{\text{if } d \geq T_{\max}} \end{cases} \quad (20)$$

*Remark 4: In Fig. 4, we show how the results in Theorem 2 highly reduce the search range $\mathcal{H}_{\mathrm{opt}}$ for the optimal values of $(t_{\mathrm{opt}}, \theta_{opt})$. However, in order to evaluate the efficiency of tightening the search range into $\mathcal{H}_{\mathrm{opt}}$, we need to evaluate the values of PL for all $(t_p, \theta_p) \in \mathcal{H}_{\mathrm{opt}}$, which is presented later in Sec. V.*

### *B. Suboptimal Solution*

From Definition 2, we recall that the value of the average path-loss between the user and the TUAV located at $p \in \mathbb{R}^3$ is

$$\mathrm{PL_p} = \left(\frac{4\pi}{\lambda}\right)^2 \left(P_{\mathrm{LoS}}(p) R_p^2 \eta_{\mathrm{LoS}} + (1 - P_{\mathrm{LoS}}(p)) R_p^2 \eta_{\mathrm{nLoS}}\right),$$

where $P_{\mathrm{LoS}}(p)$ is the LoS probability and $R_p = \sqrt{x_p^2 + y_p^2 + z_p^2}$ is the Euclidean distance. Now, by observing the above equation, we note that for a fixed value of $R_p$, $\mathrm{PL_p}$ is a decreasing function of $P_{\mathrm{LoS}}$, due to the fact that $\eta_{\mathrm{LoS}} \leq \eta_{\mathrm{NLoS}}$. Similarly, we observe that, for a fixed value of $P_{\mathrm{LoS}}$, $\mathrm{PL_p}$ is an increasing function of $R_p$. Hence, we can find a suboptimal solution by either (i) minimizing $R_p$, or (ii) maximizing $P_{\mathrm{LoS}}$. In this section, we propose a suboptimal solution to $\mathbf{OP}_2$ that is based on maximizing the $P_{\mathrm{LoS}}$. Applying the comments in Lemmas 1 and 2 to find the point $p$ within the bounds defined in Theorem 2 that maximizes the value of $P_{\mathrm{LoS}}$, we define the suboptimal values $(t_{\mathrm{sub}}, \theta_{\mathrm{sub}})$ as follows

$$(t_{\mathrm{sub}}, \theta_{\mathrm{sub}}) = \begin{cases} (\frac{d}{\cos(\theta_{\min})}, \theta_{\min}), & \text{if } d \leq T_{\max}\cos(\theta_{\min}) \\ (T_{\max}, \theta_{\min}), & \text{if } T_{\max}\cos(\theta_{\min}) \leq d \leq \mathcal{F} \\ (T_{\max}, \theta^*(T_{\max})), & \text{if } d \geq \mathcal{F}, \end{cases} \quad (21)$$

where $\mathcal{F}$ and $\theta^*$ are provided in Theorem 2. In the following theorem, we provide the suboptimal values of PL.

*Theorem 3: The suboptimal value of* PL *when the TUAV is placed at the location that maximizes* $P_{\mathrm{LoS}}$ *is*

$$\mathrm{PL}^{\mathrm{sub}} = \left(\frac{4\pi}{\lambda}\right)^2 \left(P_{\mathrm{LoS}}^{\mathrm{sub}}(R^{\mathrm{sub}})^2\eta_{\mathrm{LoS}} + (1-P_{\mathrm{LoS}}^{\mathrm{sub}})(R^{\mathrm{sub}})^2\eta_{\mathrm{nLoS}}\right), \quad (22)$$

*where*

$$P_{\mathrm{LoS}}^{\mathrm{sub}} = \begin{cases} \underbrace{a\,(90-15)^b}_{\text{if } d\le T_{\max}\cos(\theta_{\min})}, \\ \underbrace{a\left(\tan^{-1}\left(\frac{h_b+T_{\max}\sin(\theta_{\min})}{d-T_{\max}\cos(\theta_{\min})}\right)-15\right)^b}_{\text{if } T_{\max}\cos(\theta_{\min})\le d\le \mathcal{F}}, \\ \underbrace{a\left(\tan^{-1}\left(\frac{h_b\sqrt{h_b^2+d^2-T_{\max}^2}+dT_{\max}}{d\sqrt{h_b^2+d^2-T_{\max}^2}-h_bT_{\max}}\right)-15\right)^b}_{\text{if } d\ge\mathcal{F}}, \end{cases} \quad (23)$$

*and*

$$R^{\mathrm{sub}} = \begin{cases} \underbrace{h_b + d\tan(\theta_{\min})}_{\text{if } d\le T_{\max}\cos(\theta_{\min})}, \\ \underbrace{\sqrt{h_b^2+d^2+T_{\max}^2-2dT_{\max}\cos(\theta_{\min})+2h_bT_{\max}\sin(\theta_{\min})}}_{\text{if } T_{\max}\cos(\theta_{\min})\le d\le\mathcal{F}}, \\ \underbrace{\sqrt{h_b^2+d^2-T_{\max}^2}}_{\text{if } d\ge\mathcal{F}}, \end{cases} \quad (24)$$

*Proof: The above results follow directly by substituting for* $x_p = d - t_{\mathrm{sub}}\cos(\theta_{\mathrm{sub}})$, $y_p = 0$, *and* $z_p = h_b + t_{\mathrm{sub}}\sin(\theta_{\mathrm{sub}})$ *in (2) and (3).* ∎

*Corollary 3: For the case of* $\theta_{\min} = 0°$, *the results in Theorem 3 reduce to*

$$P_{\mathrm{LoS}}^{\mathrm{sub}} = \begin{cases} \underbrace{a\,(90-15)^b}_{\text{if } d\le T_{\max}}, \\ \underbrace{a\left(\tan^{-1}\left(\frac{h_b\sqrt{h_b^2+d^2-T_{\max}^2}+dT_{\max}}{d\sqrt{h_b^2+d^2-T_{\max}^2}-h_bT_{\max}}\right)-15\right)^b}_{\text{if } d\ge T_{\max}}, \end{cases} \quad (25)$$

*and*

$$R^{\mathrm{sub}} = \begin{cases} h_b, & \text{if } d\le T_{\max} \\ \sqrt{h_b^2+d^2-T_{\max}^2}, & \text{if } d\ge T_{\max}. \end{cases} \quad (26)$$

As it can be observed from Theorems 2 and 3, the value of $\theta_{\min}$ highly impacts the optimal placement of the TUAV due to inducing a minimum value on the inclination angle of the tether. Hence, in the next section, we derive the distribution of $\theta_{\min}$.

## IV. The Distribution of $\theta_{\min}$

As we recall from the definition of the hovering region, increasing the value of $\theta_{\min}$ highly reduces the mobility freedom of the TUAV and shrinks the size of the hovering region. Hence, deriving the distribution of $\theta_{\min}$ is needed due to its influence on the average value of path-loss. For that reason, we characterize the CDF of $\theta_{\min}$ in different kinds of environments such as urban, suburban, dense urban or high rise urban environments.

The value of $\theta_{\min}$ depends on the height of the rooftop ($h_b$) at which the TUAV's launching point is placed, as well as the heights of the surrounding buildings. The computation of its value highly depends on the safety regulations followed in the deployment area. In this section, we assume that if there exists a building at a distance $L < T_{\max}$ that has a height $h > h_b$ then the minimum inclination angle of the tether is $\theta_{\min} = \tan^{-1}\left(\frac{h-h_b}{L}\right)$. This assumption prevents tether tangling upon this building and ensures its safety. In order to compute the distribution of $\theta_{\min}$, we model the locations of the surrounding buildings as a Poisson point process (PPP) $\Phi_b = \{x_i\} \in \mathbb{R}^2$ with density $\beta$ building/km$^2$ [61], [62]. In addition, similar to [50], the height of each building is assumed to be Rayleigh distributed with mean $\gamma$ meters. The values of $\beta$ and $\gamma$ vary depending on the environment, as discussed in [50], as follows

$$(\beta,\gamma) = \begin{cases} (750,8), & \text{for suburban environments} \\ (500,15), & \text{for urban environments} \\ (300,20), & \text{for dense urban environments} \\ (300,50), & \text{for high rise urban environments.} \end{cases} \quad (27)$$

In the following theorem, we present the CDF of $\theta_{\min}$.

*Theorem 4: The CDF of of* $\theta_{\min}$ *is*

$$\begin{aligned} &F_{\theta_{\min}}(\theta) \\ &= \mathbb{P}(\theta_{\min}\le\theta) \\ &= \exp\left(\frac{-\pi\beta\gamma}{\tan^2(\theta)}\left(\gamma\left[\exp\left(-\frac{h_b^2}{\gamma^2}\right)\right.\right.\right. \\ &\quad \left.\left. -\exp\left(-\frac{(h_b+T_{\max}\sin(\theta))^2)}{\gamma^2}\right)\right] \\ &\quad \left.\left. -h_b\left[\Gamma\left(\frac{1}{2},\frac{(h_b+T_{\max}\sin(\theta))^2)}{\gamma^2}\right)-\Gamma(\frac{1}{2},\frac{h_b^2}{\gamma^2})\right]\right)\right), \end{aligned} \quad (28)$$

*where* $\Gamma(\bullet,\bullet)$ *is the lower incomplete Gamma function. Proof: See Appendix C.* ∎

*Remark 5: As described in detail in Appendix C, the event* $\theta_{\min} < \theta$ *takes place when every building at distance L,*

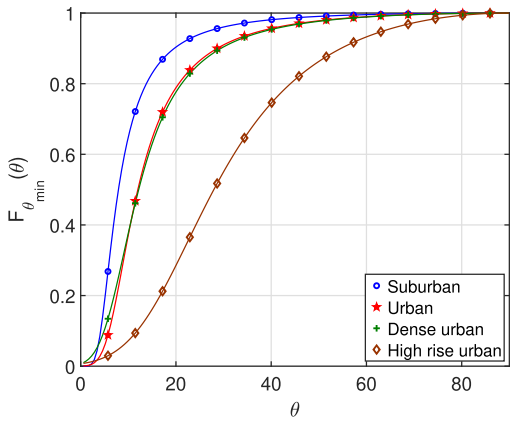


Fig. 5. The CDF of $\theta_{\min}$ for different environments.

*for any $L \leq T_{\max}\cos(\theta)$, has a height less than $h_b + L\tan(\theta)$. In other words, we only care for the heights of the buildings inside the ball $\mathcal{B}\big(0, T_{\max}\cos(\theta)\big)$. Hence, an interesting trade-off between the value of $T_{\max}$ and the CDF of $\theta_{\min}$ can be observed. In particular, at lower values of $T_{\max}$, the area of $\mathcal{B}\big(0, T_{\max}\cos(\theta)\big)$ is small. Hence, $\mathbb{P}(\theta_{\min} < \theta)$ is relatively high. However, as we increase the value of $T_{\max}$, the area of $\mathcal{B}\big(0, T_{\max}\cos(\theta)\big)$ increases, and hence, the probability decreases. The effect of this trade-off on the size of the hovering region should be carefully investigated, which is considered an interesting extension for our work.*

We plot the derived distribution of $\theta_{\min}$ in Fig. 5 for different environments while assuming that $h_b = \gamma$. Agreeing with intuition, the CDF decreases as we move from suburban to high rise urban environments. The average value of $\theta_{\min}$ can be easily computed using the CDF: $\mathbb{E}[\theta_{\min}] = \int_0^{\frac{\pi}{2}} 1 - F_{\theta_{\min}}(\theta)\mathrm{d}\theta$, which leads to the following values:

$$\mathbb{E}[\theta_{\min}] = \begin{cases} 10.6^\circ, & \text{for suburban environments} \\ 15.3^\circ, & \text{for urban environments} \\ 15.3^\circ, & \text{for dense urban environments} \\ 30.8^\circ, & \text{for high rise urban environments} \end{cases} \tag{29}$$

*Remark 6: From Fig. 5 and (29) we observe that, agreeing with intuition, the value of $\theta_{\min}$ is smaller at suburban environments due to less obstructions and shorter buildings. On the other hand, in high rise urban environments, the value of $\theta_{\min}$ is the highest. This is mainly due to the high density of tall buildings restricting the hovering region of the TUAVs.*

## V. Numerical Results and Discussion

In this section, we evaluate the results provided in this paper. In particular, we evaluate the tightness of the upper and lower bounds provided in Theorem 2, as well as the suboptimal solution provided in Theorem 3. In all the figures in this section, the optimal solution is obtained using exhaustive search, while the suboptimal results are obtained using our derived closed-form expressions. The values of the system parameters used in this section are summarized in Table III and are based on the state of the art summarized in Table I.

In Fig. 6, we show the optimal and suboptimal locations of the TUAV for different values of $d$. Given that $\theta_{\min} = 0^\circ$ and $T_{\max} = 150$, and based on our results in Theorem 2, the optimal value of the tether length is $t_{\text{opt}} = T_{\max}$ as long as $d \leq T_{\max}$. Also, the optimal value of the inclination angle is $\theta_{\text{opt}} = 0^\circ$ as long as $d \leq T_{\max}$. On the other hand, from (21), the provided suboptimal solution is $\theta_{\text{sub}} = 0^\circ$ and $t_{\text{opt}} = T_{\max}$ as long as $d \leq T_{\max}$. Hence, the optimal and suboptimal locations for the considered scenario are similar only when $d$ is less than 150. However, when $d \geq 150$, the optimal and suboptimal locations are different. We also notice that the suboptimal locations of the TUAV have significantly higher altitudes compared to the optimal locations. This behavior results from the approach used to compute the suboptimal locations, which is maximizing the LoS probability $P_{\text{LoS}}$. Given that $\theta_{\min} = 0^\circ$, the values of $t_{\text{opt}}$ and $\theta_{\text{opt}}$ should be within the bounds provided in Corollary 2, which can be easily verified using the values of $(x_{\text{opt}}, z_{\text{opt}})$ provided in Fig. 6 and the transformations $\theta_{\text{opt}} = \tan^{-1}\left(\frac{z_{\text{opt}} - h_b}{d - x_{\text{opt}}}\right)$ and $t_{\text{opt}} = \sqrt{(z - h_b)^2 + (d - x_{\text{opt}})^2}$.

TABLE III
Simulation Parameters

| parameter | value | parameter | value |
|---|---|---|---|
| $T_{\max}$ | 150 m | $a$, $b$ | 0.37, 0.21 |
| $h_b$ | 30 m | $\eta_{\text{LoS}}$ | 1.6 dBs |
| $\theta_{\min}$ | $0^\circ$ | $\eta_{\text{nLoS}}$ | $= 23$ dBs |

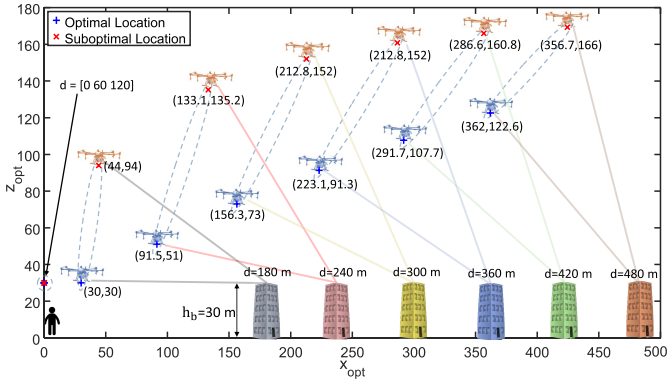


Fig. 6. The optimal and suboptimal locations of the TUAV as we increase the value of $d$.

In Theorem 2, we provided upper and lower bounds for the optimal values of the tether length and inclination angle $(t_{\text{opt}}, \theta_{\text{opt}})$. To verify these bounds, we provide the values of $\theta_{\text{opt}}$ and $t_{\text{opt}}$ for different values of $\theta_{\min}$ in Figures 7 and 8. In each figure, we also show the upper and the lower bounds provided in Theorem 2. The results prove that $(\theta_{\text{opt}}, t_{\text{opt}}) \in \mathcal{H}_{\text{opt}}$, which is provided in Theorem 2. In addition, given that $\mathcal{F} = 150$ when $\theta_{\min} = 0^\circ$, $\mathcal{F} = 163$ when $\theta_{\min} = 15^\circ$, and $\mathcal{F} = 190$ when $\theta_{\min} = 30^\circ$, we observe that the upper and lower bounds of $\theta_{\text{opt}}$ only deviate when $d \geq \mathcal{F}$, which agrees with our results in Theorem 2. Similarly, also agreeing with Theorem 2, we observe that the upper and lower bounds of $t_{\text{opt}}$ are both equal to $T_{\max}$ when $d \geq \mathcal{F}$.

In Fig. 9, we compare the optimal values of $\theta_{\text{opt}}$ to the suboptimal values provided in (21). As expected, since the suboptimal solution aims to maximize the value of $P_{\text{LoS}}$, we can observe that $\theta_{\text{sub}} > \theta_{\text{opt}}$. This is also evident from the definitions of $\theta_{\text{opt}}$ in Theorem 2 and $\theta_{\text{sub}}$ in (21),

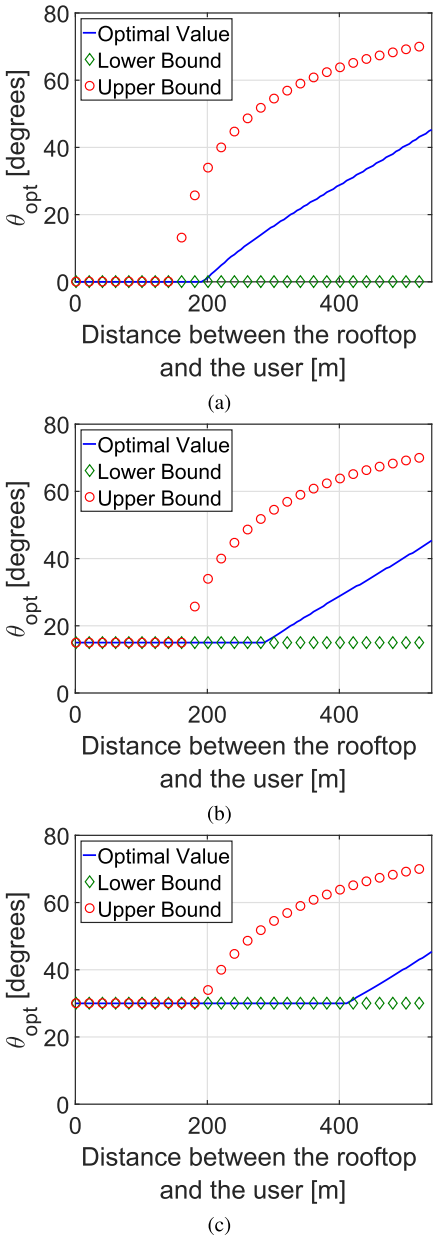


Fig. 7. The optimal value of $\theta$ is always within the bounds derived in Theorem 2 for (a) $\theta_{\min} = 0°$, (b) $\theta_{\min} = 15°$, and (c) $\theta_{\min} = 30°$.

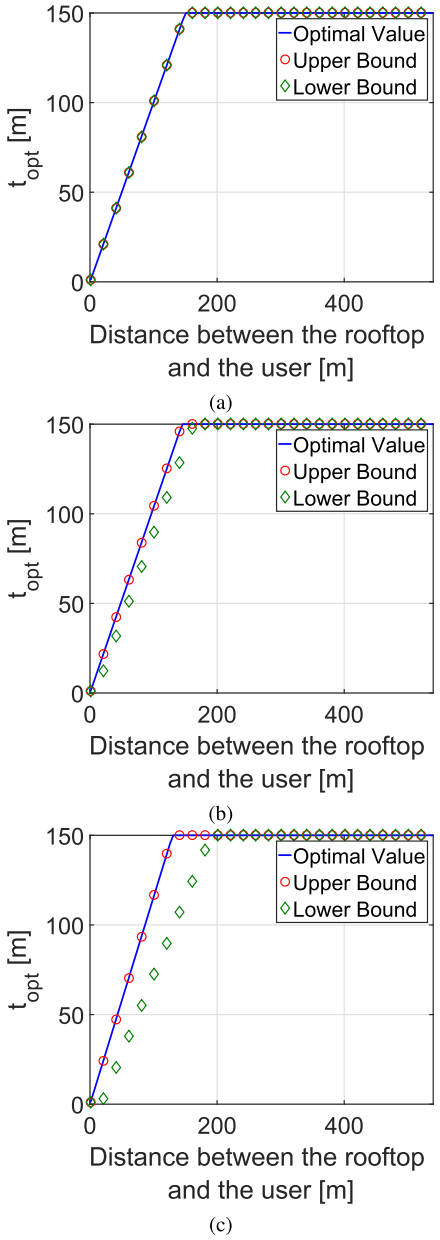


Fig. 8. The optimal value of $t$ is always within the bounds derived in Theorem 2 for (a) $\theta_{\min} = 0°$, (b) $\theta_{\min} = 15°$, and (c) $\theta_{\min} = 30°$.

where, as shown in Fig. 9, $\theta_{\text{sub}} = \theta_{\text{opt}} = \theta_{\min}$ when $d \leq \mathcal{F}$. On the other hand, $\theta_{\min} \leq \theta_{\text{opt}} \leq \theta_{\text{sub}}$ when $d \geq \mathcal{F}$. To evaluate the tightness of the proposed suboptimal solution, we have to compare the values of PL, which is discussed next.

In Fig. 10, we plot the optimal and suboptimal values of PL, for different values of $T_{\max}$. The results show that the gain from increasing the maximum tether length can be up to 10 dBs reduction in the optimal value of the PL at lower values of $d$. However, as $d$ increases, the effect of increasing the value of $T_{\max}$ decreases. This behavior reflects some useful insights about the benefits of increasing the value of $T_{\max}$. When the intended users are located closer to the building, increasing the maximum tether length is very beneficial. However, if the users are located far away from the building, the effect of increasing $T_{\max}$ reduces. Note that value of $T_{\max}$ relies on lots of aspects related to the ability to control the tether tension and support its weight. That is why the value of $T_{\max}$ is currently limited by 150 meters in most of the commercially available TUAV products.

As stated in Remark 4, we need to evaluate how efficient are the bounds provided in Theorem 2. For that purpose, we define the *PL range* as the values of $PL_p \forall p \in \mathcal{H}_{\text{opt}}$, where $\mathcal{H}_{\text{opt}}$ is provided in Theorem 2. We plot this PL range for different values of $d$ with $\theta_{\min} = 0°$ in Fig. 11a, $\theta_{\min} = 15°$ in Fig. 11b, and $\theta_{\min} = 30°$ in Fig. 11c. We also plot the suboptimal value of PL, proposed in Theorem 3. The results show the tightness of the PL range for all the points within the bounds provided in Theorem 2. In addition, the results show that the suboptimal solution is less than 3dBs over the optimal value for the case of $\theta_{\min} = 15°$, and it gets even tighter as $\theta_{\min}$ increases.

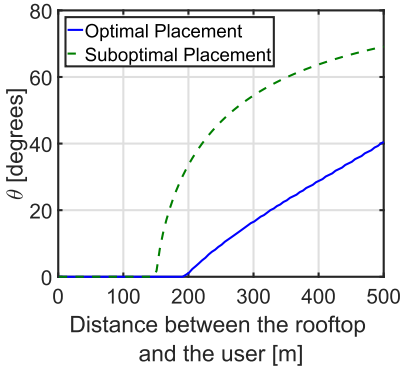


(a)

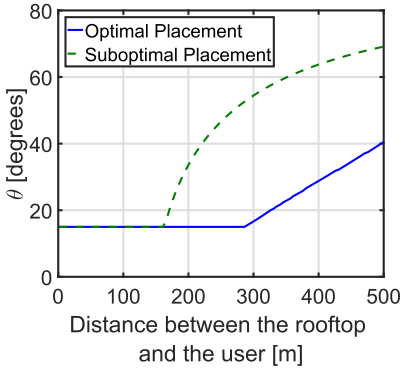


(b)

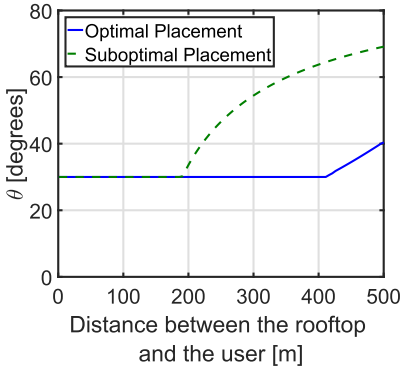


(c)

Fig. 9. Optimal and suboptimal values of $\theta$ for different values of $d$: (a) $\theta_{\min} = 0°$, (b) $\theta_{\min} = 15°$, and (c) $\theta_{\min} = 30°$.

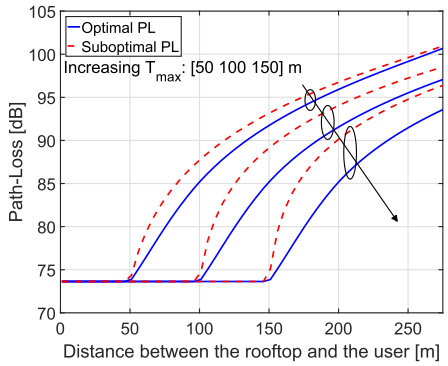


Fig. 10. Optimal and suboptimal values of PL for different values of $d$ and $T_{\max}$.

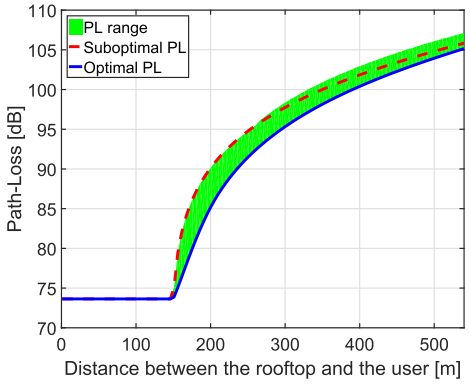


(a)

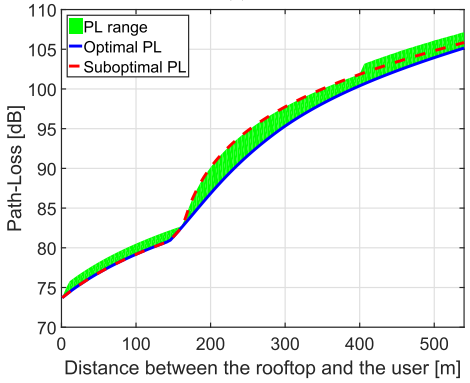


(b)

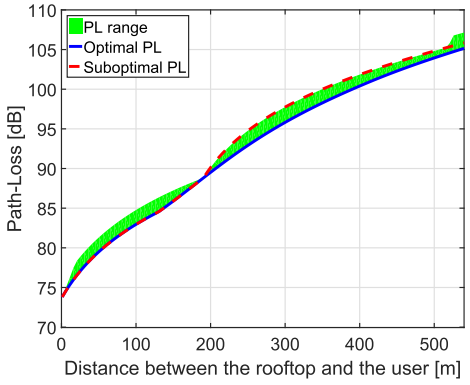


(c)

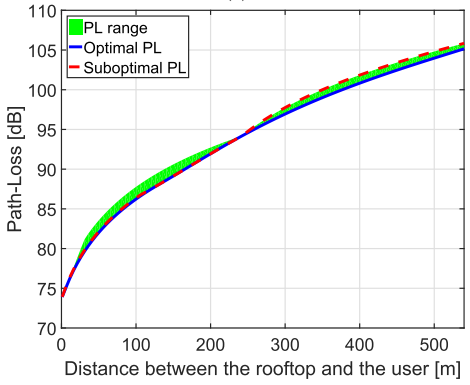


(d)

Fig. 11. The PL range against different values of $d$ for: (a) $\theta_{\min} = 0°$, (b) $\theta_{\min} = 15°$, (c) $\theta_{\min} = 30°$, and (d) $\theta_{\min} = 45°$.

The results provided in Fig. 11 show how the limited tether length leads to additional path-loss as the user gets further from the rooftop. In particular, as stated briefly in the introduction, in the case of untethered UAVs, the problem considered in this paper would be solved simply by deploying

the UAV right above the user. Hence, the case of $d = 0$ in Fig. 11 represents the average path-loss when an untethered UAV is used. Clearly, as the distance between the user and the rooftop increases, the extra path-loss caused by the tether reaches up to 30 dBs.

## VI. Conclusion and Future Work

In this paper, we developed the first mathematical model for the deployment problem of a TUAV-enabled communication system. In particular, we considered a system of a TUAV whose launching point is placed on the rooftop of a building, and a target receiver located at distance $d$ from the building. For this setup, we first formally defined the hovering region of the TUAV, which is the set of locations achievable by the TUAV, given the tether maximum length and minimum inclination angle. Next, we used the mathematical model for the hovering region as a constraint for the optimal deployment problem. We derived upper and lower bounds for the optimal tether length and inclination angles, in order to minimize the average path-loss. In addition, we provided a closed-form expression for a suboptimal solution to the deployment problem, which maximizes the LoS probability. Using simulation results, assuming a dense urban environment, we showed the tightness of the derived upper and lower bounds, as well as the proposed suboptimal solution, in terms of average path-loss value. Finally, using tools from stochastic geometry, we derived the probability distribution of the minimum inclination angle of the tether, which highly depends on the density of the surrounding buildings and their altitudes, to avoid accidental tangling. We showed that the expected value of the minimum inclination angle increases as we move from suburban regions to high rise urban regions.

The research in the area of TUAV-enabled communication systems, in terms of analysis and design, is still taking its first steps. Hence, this work has many potential extensions. For instance, the placement of TUAVs in user hotspots with multiple users and known user distribution should be well investigated. In particular, given the tether length, the location of the rooftop with respect to the center of the hotspot, and the user distribution in the hotspot, the optimal tether length and inclination angle should be derived.

Given the continuous change in the user spatial distribution with time, the TUAV's optimal location actually changes with time. Hence, to study a TUAV-enabled cellular network, spatio-temporal analysis should be provided that captures the change in traffic demand both in time and space, which is another potential extension to this work.

## Appendix A
## Proof of Lemma 1

For a given $\theta_p$, we can write $R_p^2$ as follows

$$R_p^2 = x_p^2 + z_p^2 = (d - t_p\cos(\theta_p))^2 + (h_b + t_p\sin(\theta_p))^2 = d^2 + h_b^2 + t_p^2 - 2dt_p\cos(\theta_p) + 2h_b t_p\sin(\theta_p). \quad (30)$$

The above function's second derivative with respect to $t_p$ is positive, hence, it is a convex function, which means that $R_p$ is also a convex function of $t_p$. Its minimum value can be found by equalizing the first derivative to zero, which leads to the final expression of $t^*$ provided in the first part of the Lemma.

To prove that $P_{\text{LoS}}$ is an increasing function of $t_p$, we just need to show that the fraction $\frac{z_p}{x_p}$ is an increasing function of $t_p$. This is because, recalling (3), $P_{\text{LoS}}$ is an increasing function of the fraction $\frac{z_p}{x_p}$. This fraction can be written as follows

$$\frac{z_p}{x_p} = \frac{h_b + t_p\sin(\theta_p)}{d - t_p\cos(\theta_p)}, \quad (31)$$

which is an increasing function of $t_p$ in the range $0 < \theta_p < \frac{\pi}{2}$. This concludes the proof.

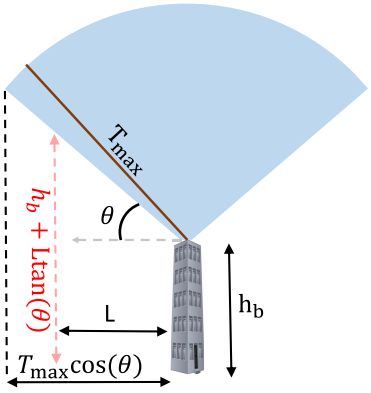


Fig. 12. For a given value of $\theta$, only the heights of the buildings inside the ball $\mathcal{B}(0, T_{\max}\cos(\theta))$ affect the value of $\mathbb{P}(\theta_{\min} \leq \theta)$.

## Appendix B
## Proof of Lemma 2

Given that $0 < \theta_p < \frac{\pi}{2}$, we can easily observe that $R_p^2$ in (30) in Appendix A is an increasing function of $\theta_p$.

As stated in Appendix A, $P_{\text{LoS}}$ is an increasing function of the fraction $\frac{z_p}{x_p}$, which means that we only need to prove the concavity of $\frac{z_p}{x_p}$ as a function of $\theta_p$. Given that $\frac{z_p}{x_p} = \frac{h_b + t_p\sin(\theta_p)}{d - t_p\cos(\theta_p)}$, the first derivative is

$$\frac{t_p\cos(\theta_p)(d - t_p\cos(\theta_p)) - t_p\sin(\theta_p)(h_b + t_p\sin(\theta_p))}{(d - t_p\cos(\theta_p))^2} = \frac{t_p(d\cos(\theta_p) - h_b\sin(\theta_p) - t_p)}{(d - t_p\cos(\theta_p))^2}. \quad (32)$$

The first derivative in (32) is a decreasing function of $\theta_p$ in the range $0 < \theta_p < \frac{\pi}{2}$, which implies the concavity of $\frac{z_p}{x_p}$. The value of $\theta_p$ that maximizes $\frac{z_p}{x_p}$ can be found by equalizing the first derivative to zero, which leads to $\theta^*$ as defined in Lemma 2.

## Appendix C
## Proof of Theorem 4

As shown in Fig. 12, assuming that the TUAV's rooftop is located at the origin, in order to ensure that $\theta_{\min} < \theta$, we need to ensure that any building at distance $L$ from the origin, inside the ball $\mathcal{B}(0, T_{\max}\cos(\theta))$, has a height $h_L < h_b + L\tan(\theta)$.

Hence the CDF of $\theta_{\min}$ can be derived as follows

$$\mathbb{P}(\theta_{\min} \leq \theta) = \mathbb{P}\left( \bigcap_{x_i \in \Phi_b \cap \mathcal{B}(0, T_{\max}\cos(\theta))} h_{x_i} < h_b + |x_i| \tan(\theta) \right), \quad (33)$$

where $h_{x_i}$ is the height of the building located at $x_i$. Given that the set of heights $\{h_{x_i}\}$ are i.i.d with Rayleigh distribution and mean $\gamma$ then

$$\begin{aligned}
&\mathbb{P}(\theta_{\min} \leq \theta) \\
&= \mathbb{E}_{\Phi_b}\left[ \prod_{x_i \in \Phi_b \cap \mathcal{B}(0, T_{\max}\cos(\theta))} \mathbb{P}\left(h_{x_i} < h_b + |x_i| \tan(\theta)\right) \right] \\
&= \mathbb{E}_{\Phi_b}\Bigg[ \prod_{x_i \in \Phi_b \cap \mathcal{B}(0, T_{\max}\cos(\theta))} (1 \\
&\quad - \exp\left( \frac{-(h_b + |x_i| \tan(\theta))^2}{\gamma^2} \right) \Bigg) \Bigg] \\
&\overset{(a)}{=} \exp\left( -2\pi\beta \int_0^{T_{\max}\cos(\theta)} \exp\left( \frac{-(h_b + r\tan(\theta))^2}{\gamma^2} \right) r \mathrm{d}r \right),
\end{aligned} \quad (34)$$

where $(a)$ results from using the probability generating functional (PGFL) of PPP [63]. Applying simple algebraic manipulations to the expression in (34) leads to the final result in Theorem 4.

## REFERENCES


[1] M. Mozaffari, W. Saad, M. Bennis, Y.-H. Nam, and M. Debbah, "A tutorial on UAVs for wireless networks: Applications, challenges, and open problems," *IEEE Commun. Surveys Tuts.*, vol. 21, no. 3, pp. 2334–2360, 3rd Quart., 2019.

[2] A. Fotouhi *et al.*, "Survey on UAV cellular communications: Practical aspects, standardization advancements, regulation, and security challenges," *IEEE Commun. Surveys Tuts.*, vol. 21, no. 4, pp. 3417–3442, Mar. 2019.

[3] X. Cao, P. Yang, M. Alzenad, X. Xi, D. Wu, and H. Yanikomeroglu, "Airborne communication networks: A survey," *IEEE J. Sel. Areas Commun.*, vol. 36, no. 9, pp. 1907–1926, Sep. 2018.

[4] Y. Zeng, Q. Wu, and R. Zhang, "Accessing from the sky: A tutorial on UAV communications for 5G and beyond," 2019, *arXiv:1903.05289*. [Online]. Available: http://arxiv.org/abs/1903.05289

[5] B. Li, Z. Fei, and Y. Zhang, "UAV communications for 5G and beyond: Recent advances and future trends," *IEEE Internet Things J.*, vol. 6, no. 2, pp. 2241–2263, Apr. 2019.

[6] S. D. Muruganathan *et al.*, "An overview of 3GPP release-15 study on enhanced LTE support for connected drones," 2018, *arXiv:1805.00826*. [Online]. Available: http://arxiv.org/abs/1805.00826

[7] R. Amer, W. Saad, and N. Marchetti, "Mobility in the sky: Performance and mobility analysis for cellular-connected UAVs," 2019, *arXiv:1908.07774*. [Online]. Available: http://arxiv.org/abs/1908.07774

[8] M. M. Azari, F. Rosas, and S. Pollin, "Cellular connectivity for UAVs: Network modeling, performance analysis, and design guidelines," *IEEE Trans. Wireless Commun.*, vol. 18, no. 7, pp. 3366–3381, Jul. 2019.

[9] Y. Zeng, J. Lyu, and R. Zhang, "Cellular-connected UAV: Potential, challenges, and promising technologies," *IEEE Wireless Commun.*, vol. 26, no. 1, pp. 120–127, Feb. 2019.

[10] M. Mahdi Azari, G. Geraci, A. Garcia-Rodriguez, and S. Pollin, "Cellular UAV-to-UAV communications," 2019, *arXiv:1904.05104*. [Online]. Available: http://arxiv.org/abs/1904.05104

[11] X. Lin *et al.*, "The sky is not the limit: LTE for unmanned aerial vehicles," *IEEE Commun. Mag.*, vol. 56, no. 4, pp. 204–210, Apr. 2018.

[12] G. Geraci, A. Garcia-Rodriguez, L. Galati Giordano, D. Lopez-Perez, and E. Bjornson, "Understanding UAV cellular communications: From existing networks to massive MIMO," *IEEE Access*, vol. 6, pp. 67853–67865, 2018.

[13] R. Amer, W. Saad, and N. Marchetti, "Towards a connected sky: Performance of beamforming with down-tilted antennas for ground and UAV user co-existence," 2019, *arXiv:1907.05085*. [Online]. Available: http://arxiv.org/abs/1907.05085

[14] H. Wu, X. Tao, N. Zhang, and X. Shen, "Cooperative UAV cluster-assisted terrestrial cellular networks for ubiquitous coverage," *IEEE J. Sel. Areas Commun.*, vol. 36, no. 9, pp. 2045–2058, Sep. 2018.

[15] Z. Xiao, P. Xia, and X.-G. Xia, "Enabling UAV cellular with millimeter-wave communication: Potentials and approaches," *IEEE Commun. Mag.*, vol. 54, no. 5, pp. 66–73, May 2016.

[16] P. Yang, X. Cao, C. Yin, Z. Xiao, X. Xi, and D. Wu, "Proactive drone-cell deployment: Overload relief for a cellular network under flash crowd traffic," *IEEE Trans. Intell. Transp. Syst.*, vol. 18, no. 10, pp. 2877–2892, Oct. 2017.

[17] Y. Zeng, R. Zhang, and T. J. Lim, "Wireless communications with unmanned aerial vehicles: Opportunities and challenges," *IEEE Commun. Mag.*, vol. 54, no. 5, pp. 36–42, May 2016.

[18] M.-A. Lahmeri, M. A. Kishk, and M.-S. Alouini, "Stochastic geometry-based analysis of airborne base stations with laser-powered UAVs," *IEEE Commun. Lett.*, vol. 24, no. 1, pp. 173–177, Jan. 2020.

[19] I. Bor-Yaliniz and H. Yanikomeroglu, "The new frontier in RAN heterogeneity: Multi-tier drone-cells," *IEEE Commun. Mag.*, vol. 54, no. 11, pp. 48–55, Nov. 2016.

[20] A. M. Hayajneh, S. A. R. Zaidi, D. C. McLernon, M. Di Renzo, and M. Ghogho, "Performance analysis of UAV enabled disaster recovery networks: A stochastic geometric framework based on cluster processes," *IEEE Access*, vol. 6, pp. 26215–26230, 2018.

[21] P. K. Sharma and D. I. Kim, "Random 3D mobile UAV networks: Mobility modeling and coverage probability," *IEEE Trans. Wireless Commun.*, vol. 18, no. 5, pp. 2527–2538, May 2019.

[22] M. Banagar and H. S. Dhillon, "Performance characterization of canonical mobility models in drone cellular networks," 2019, *arXiv:1908.05243*. [Online]. Available: http://arxiv.org/abs/1908.05243

[23] Y. Zeng and R. Zhang, "Energy-efficient UAV communication with trajectory optimization," *IEEE Trans. Wireless Commun.*, vol. 16, no. 6, pp. 3747–3760, Jun. 2017.

[24] A. Fotouhi, M. Ding, and M. Hassan, "Flying drone base stations for macro hotspots," *IEEE Access*, vol. 6, pp. 19530–19539, 2018.

[25] M. A. Abd-Elmagid and H. S. Dhillon, "Average peak age-of-information minimization in UAV-assisted IoT networks," *IEEE Trans. Veh. Technol.*, vol. 68, no. 2, pp. 2003–2008, Feb. 2019.

[26] Q. Wu, Y. Zeng, and R. Zhang, "Joint trajectory and communication design for multi-UAV enabled wireless networks," *IEEE Trans. Wireless Commun.*, vol. 17, no. 3, pp. 2109–2121, Mar. 2018.

[27] J. Lyu, Y. Zeng, and R. Zhang, "Cyclical multiple access in UAV-aided communications: A throughput-delay tradeoff," *IEEE Wireless Commun. Lett.*, vol. 5, no. 6, pp. 600–603, Dec. 2016.

[28] M. Mozaffari, W. Saad, M. Bennis, and M. Debbah, "Wireless communication using unmanned aerial vehicles (UAVs): Optimal transport theory for hover time optimization," *IEEE Trans. Wireless Commun.*, vol. 16, no. 12, pp. 8052–8066, Dec. 2017.

[29] V. V. Chetlur and H. S. Dhillon, "Downlink coverage analysis for a finite 3D wireless network of unmanned aerial vehicles," *IEEE Trans. Commun.*, vol. 65, no. 10, pp. 4543–4558, Oct. 2017.

[30] M. Mozaffari, W. Saad, M. Bennis, and M. Debbah, "Unmanned aerial vehicle with underlaid device-to-device communications: Performance and tradeoffs," *IEEE Trans. Wireless Commun.*, vol. 15, no. 6, pp. 3949–3963, Jun. 2016.

[31] K. Dorling, J. Heinrichs, G. G. Messier, and S. Magierowski, "Vehicle routing problems for drone delivery," *IEEE Trans. Syst., Man, Cybern., Syst.*, vol. 47, no. 1, pp. 70–85, Jan. 2017.

[32] A. Thibbotuwawa, P. Nielsen, B. Zbigniew, and G. Bocewicz, "Energy consumption in unmanned aerial vehicles: A review of energy consumption models and their relation to the UAV routing," in *Proc. 39th Int. Conf. Inf. Syst. Archit. Technol.* Cham, Switzerland: Springer, 2018, pp. 173–184.

[33] D. Jones. (2019). *Power Consumption: 5G Basestations Are Hungry, Hungry Hippos*. Accessed: Jan. 22, 2020. [Online]. Available: https://t2m.io/GTyT8Wgo

[34] T. Long, M. Ozger, O. Cetinkaya, and O. B. Akan, "Energy neutral Internet of drones," *IEEE Commun. Mag.*, vol. 56, no. 1, pp. 22–28, Jan. 2018.

[35] B. Galkin, J. Kibilda, and L. A. DaSilva, "UAVs as mobile infrastructure: Addressing battery lifetime," *IEEE Commun. Mag.*, vol. 57, no. 6, pp. 132–137, Jun. 2019.
[36] M. A. Kishk, A. Bader, and M.-S. Alouini, "Capacity and coverage enhancement using long-endurance tethered airborne base stations," 2019, *arXiv:1906.11559*. [Online]. Available: http://arxiv.org/abs/1906.11559
[37] M. Alzenad, M. Z. Shakir, H. Yanikomeroglu, and M.-S. Alouini, "FSO-based vertical Backhaul/Fronthaul framework for 5G+ wireless networks," *IEEE Commun. Mag.*, vol. 56, no. 1, pp. 218–224, Jan. 2018.
[38] S. Chandrasekharan *et al.*, "Designing and implementing future aerial communication networks," *IEEE Commun. Mag.*, vol. 54, no. 5, pp. 26–34, May 2016.
[39] C. Tugrul Cicek, H. Gultekin, B. Tavli, and H. Yanikomeroglu, "Backhaul-aware optimization of UAV base station location and bandwidth allocation for profit maximization," 2018, *arXiv:1810.12395*. [Online]. Available: http://arxiv.org/abs/1810.12395
[40] B. Galkin, J. Kibilda, and L. A. DaSilva, "Backhaul for low-altitude UAVs in urban environments," in *Proc. IEEE Int. Conf. Commun. (ICC)*, May 2018, pp. 1–6.
[41] K. Sundaresan, E. Chai, A. Chakraborty, and S. Rangarajan, "SkyLiTE: End-to-end design of low-altitude UAV networks for providing LTE connectivity," 2018, *arXiv:1802.06042*. [Online]. Available: http://arxiv.org/abs/1802.06042
[42] Equinox Innovative Systems. (2017). *DELTA 3C: Tri-Sector Cell Tower*. Accessed: Jan. 22, 2020. [Online]. Available: https://t2m.io/UaF8ZYbq
[43] Tethered Drone Systems. (2019). *Tethered Drone Systems: The Future of Tethered UAV Technology*. Accessed: Jan. 22, 2020. [Online]. Available: https://t2m.io/eMsFWd5P
[44] Aria Insights. *PARC: The Future of High-Powered Commercial Drones*. Accessed: Jan. 22, 2020. [Online]. Available: https://t2m.io/bufh6WRy
[45] Elistair. (2014). *Orion: Persistent UAV for Surveillence and Communications*. Accessed: Jan. 22, 2020. [Online]. Available: https://t2m.io/5LeDMh9S
[46] European Union FP7. (2019). *ABSOLUTE—Aerial Base Stations With Opportunistic Links for Unexpected & Temporary Events*. Accessed: Jan. 22, 2020. [Online]. Available: https://t2m.io/RbeVUhSr
[47] M. Banagar and H. S. Dhillon, "3GPP-inspired stochastic geometry-based mobility model for a drone cellular network," in *Proc. IEEE Global Commun. Conf. (GLOBECOM)*, Dec. 2019, pp. 1–6.
[48] M. Y. Selim and A. E. Kamal, "Post-disaster 4G/5G network rehabilitation using drones: Solving battery and backhaul issues," in *Proc. IEEE Globecom Workshops (GC Wkshps)*, Dec. 2018, pp. 1–6.
[49] Q. Wu, J. Xu, and R. Zhang, "Capacity characterization of UAV-enabled two-user broadcast channel," *IEEE J. Sel. Areas Commun.*, vol. 36, no. 9, pp. 1955–1971, Sep. 2018.
[50] A. Al-Hourani, S. Kandeepan, and S. Lardner, "Optimal LAP altitude for maximum coverage," *IEEE Wireless Commun. Lett.*, vol. 3, no. 6, pp. 569–572, Dec. 2014.
[51] M. Alzenad, A. El-Keyi, F. Lagum, and H. Yanikomeroglu, "3-D placement of an unmanned aerial vehicle base station (UAV-BS) for energy-efficient maximal coverage," *IEEE Wireless Commun. Lett.*, vol. 6, no. 4, pp. 434–437, Aug. 2017.
[52] J. Lyu, Y. Zeng, R. Zhang, and T. J. Lim, "Placement optimization of UAV-mounted mobile base stations," *IEEE Commun. Lett.*, vol. 21, no. 3, pp. 604–607, Mar. 2017.
[53] M. Mozaffari, W. Saad, M. Bennis, and M. Debbah, "Efficient deployment of multiple unmanned aerial vehicles for optimal wireless coverage," *IEEE Commun. Lett.*, vol. 20, no. 8, pp. 1647–1650, Aug. 2016.
[54] R. I. Bor-Yaliniz, A. El-Keyi, and H. Yanikomeroglu, "Efficient 3-D placement of an aerial base station in next generation cellular networks," in *Proc. IEEE Int. Conf. Commun. (ICC)*, May 2016, pp. 1–5.
[55] M. Mozaffari, W. Saad, M. Bennis, and M. Debbah, "Mobile unmanned aerial vehicles (UAVs) for energy-efficient Internet of Things communications," *IEEE Trans. Wireless Commun.*, vol. 16, no. 11, pp. 7574–7589, Nov. 2017.
[56] O. M. Bushnaq, A. Celik, H. Elsawy, M.-S. Alouini, and T. Y. Al-Naffouri, "Aeronautical data aggregation and field estimation in IoT networks: Hovering and traveling time dilemma of UAVs," *IEEE Trans. Wireless Commun.*, vol. 18, no. 10, pp. 4620–4635, Oct. 2019.
[57] B. Galkin, J. Kibilda, and L. A. DaSilva, "A stochastic model for UAV networks positioned above demand hotspots in urban environments," *IEEE Trans. Veh. Technol.*, vol. 68, no. 7, pp. 6985–6996, Jul. 2019.
[58] W. Yi, Y. Liu, E. Bodanese, A. Nallanathan, and G. K. Karagiannidis, "A unified spatial framework for UAV-aided mmWave networks," *IEEE Trans. Commun.*, vol. 67, no. 12, pp. 8801–8817, Dec. 2019.
[59] T. Hou, Y. Liu, Z. Song, X. Sun, and Y. Chen, "Exploiting NOMA for UAV communications in large-scale cellular networks," *IEEE Trans. Commun.*, vol. 67, no. 10, pp. 6897–6911, Oct. 2019.
[60] A. Al-Hourani, S. Kandeepan, and A. Jamalipour, "Modeling air-to-ground path loss for low altitude platforms in urban environments," in *Proc. IEEE Global Commun. Conf.*, Dec. 2014, pp. 2898–2904.
[61] T. Bai, R. Vaze, and R. W. Heath, Jr., "Analysis of blockage effects on urban cellular networks," *IEEE Trans. Wireless Commun.*, vol. 13, no. 9, pp. 5070–5083, Sep. 2014.
[62] A. K. Gupta, J. G. Andrews, and R. W. Heath, Jr., "Macrodiversity in cellular networks with random blockages," *IEEE Trans. Wireless Commun.*, vol. 17, no. 2, pp. 996–1010, Feb. 2018.
[63] M. Haenggi, *Stochastic Geometry for Wireless Networks*. Cambridge, U.K.: Cambridge Univ. Press, 2012.

**Mustafa A. Kishk** (Member, IEEE) received the B.Sc. and M.Sc. degrees from Cairo University in 2013 and 2015, respectively, and the Ph.D. degree from Virginia Tech in 2018. He is currently a Post-Doctoral Research Fellow with the Communication Theory Laboratory, King Abdullah University of Science and Technology (KAUST). His current research interests include stochastic geometry, energy harvesting wireless networks, UAV-enabled communication systems, and satellite communications.

**Ahmed Bader** (Senior Member, IEEE) received the B.S. degree from the University of Jordan in 2003, the M.S. degree from The Ohio State University in 2006, and the Ph.D. degree from Telecom ParisTech, France, in 2013, all in electrical engineering. He has more than ten years of experience in the wireless industry and has previously held positions at Emerson and Siemens. Since 2013, he has been with the King Abdullah University of Science and Technology (KAUST), Saudi Arabia, where he is spearheading multiple applied research projects that have led to several patent-pending technologies. He is also a Co-Founder of Insyab Wireless, a Dubai-based company designing real-time connectivity solutions for unmanned systems. His research interests are mainly in the domain of large-scale wireless networks.

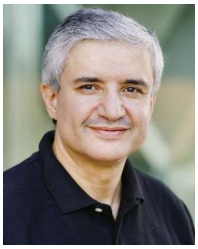

**Mohamed-Slim Alouini** (Fellow, IEEE) was born in Tunis, Tunisia. He received the Ph.D. degree in electrical engineering from the California Institute of Technology (Caltech), Pasadena, CA, USA, in 1998. He has served as a Faculty Member with the University of Minnesota, Minneapolis, MN, USA, then in the Texas A&M University, Qatar, Education City, Doha, Qatar, before joining the King Abdullah University of Science and Technology (KAUST), Thuwal, Saudi Arabia, as a Professor of electrical engineering, in 2009. His current research interests include the modeling, design, and performance analysis of wireless communication systems.